Nanoscale

PAPER

View Article Online
View Journal | View Issue

Cite this: *Nanoscale*, 2025, **17**, 17256

Investigation on thyroglobulin and myoglobin using graphene-enhanced Raman spectroscopy as a tool†

Anamika Sharma and Venkata Ramanaiah Dantham *

Received 22nd February 2025,
Accepted 30th June 2025

DOI: 10.1039/d5nr00800j

rsc.li/nanoscale

Herein, for the first time, we report the experimental investigation on thyroglobulin (Tg) and myoglobin (Mb) using graphene-enhanced Raman spectroscopy as a tool. Tg is the protein precursor of thyroid hormones, while Mb can be used as an early cardiac protein biomarker. In the beginning, the absorption properties of Tg and Mb are investigated with the help of a UV-visible spectrophotometer. Later, Tg and Mb are dispersed over two different glass substrates by drop-casting 10 μL of protein solutions with a concentration of 1 μM and their conventional Raman scattering (CRS) spectra are recorded. However, none of the vibrational modes are significant in their CRS spectra. Therefore, the graphene-enhanced Raman scattering (GERS) spectra of Tg and Mb are recorded with a high signal-to-noise ratio. The number and intensity of the vibrational modes in the GERS spectra are found to strongly depend upon the probed location. Finally, the assignment of all the observed vibrational modes is performed.

1. Introduction

The crucial functions of biological macromolecules in our daily activities create a growing need for the identification and quantitative analysis of biomolecules, including proteins, nucleic acids, lipids, and carbohydrates. Proteins are essential biomolecules that play a vital role in all biological processes, including DNA replication, catalyzing metabolic reactions, and transporting molecules to different locations.[1] Therefore, understanding the structural dynamics and molecular interactions of complex biomolecules containing proteins is of great interest in various research areas ranging from molecular biology to biophysics, medicine, and biotechnology.

Raman spectroscopy is an essential tool for label-free, non-invasive, highly sensitive, and real-time monitoring of biological samples, playing a crucial role in the early-stage detection and diagnosis of various dangerous diseases.[2–5] A few studies have demonstrated the Raman spectroscopy of protein biomarkers.[6] The true potential of Raman spectroscopy in protein research is limited due to low Raman signal and fluorescence interference from biological samples.[7,8] Several advanced techniques, including surface-enhanced Raman scattering (SERS), photonic nanojet (PNJ)-mediated SERS, resonance Raman spectroscopy, PNJ-assisted Raman microscopy, whispering gallery mode (WGM)-assisted Raman microscopy, and graphene-enhanced Raman scattering (GERS), have been adopted to enhance weak Raman signals from different materials.[8–17]

In the SERS technique, two main mechanisms contribute to the Raman signal enhancement: the electromagnetic mechanism (EM) and the chemical mechanism (CM). In the SERS technique, when metallic substrates are utilized, the EM and CM contribute to the Raman signal enhancement. However, in the case of graphene-based substrates, the enhancement is primarily attributed to the CM rather than the EM.[16,18] This is because the monolayer graphene films (MGFs) have an optical absorption of nearly 2.3% in the UV-visible region, and surface plasmons are excited in the terahertz frequency range rather than in the visible range.[19–24] The GERS technique represents an advancement over the conventional SERS technique. It effectively suppresses fluorescence and creates an optimal environment for molecular interactions, resulting in an enhanced Raman signal for delicate biomolecules, pesticides, dyes, and more. It is widely applicable in the systematic study of protein molecules due to graphene's exceptional features, such as uniform surface area, fluorescence quenching, chemical stability, biocompatibility, and high optical transmission.[16,25–30] It provides a simple, reliable, and inexpensive platform for protein molecules to interact with MGFs to obtain fingerprint characteristics with a superior signal-to-noise ratio (S/N), even for small amounts of protein biomarkers.[31–37] The GERS technique relies solely on the CM, providing insight into the molecular interactions between the analyte molecule and the MGF. These advantages highlight

Department of Physics, Indian Institute of Technology Patna, Bihar, India, 801103.
E-mail: dantham@iitp.ac.in

† Electronic supplementary information (ESI) available. See DOI: https://doi.org/10.1039/d5nr00800j

the superiority of the GERS technique over the SERS technique. This makes the GERS technique a powerful tool for studying protein molecules in their native biological conditions. The GERS technique has been successfully used to detect protein biomarkers such as hemoglobin, albumin, adenosine, *etc*.[8,38] However, it is important to note that the enhancement of the Raman signal is always lower in the GERS technique relative to the conventional SERS technique due to its reliance on the CM rather than the EM. This can be considered a limitation of the GERS technique over the conventional SERS technique. Protein biomarkers, which contain organic components such as aromatic amino acids, aliphatic side chains, and aromatic residues, can chemically bind to the graphene surface through π–π stacking interactions. This binding provides valuable insights into the molecular orientation, spectral variability, and charge transfer behavior within the protein–graphene system.[39,40] This technique has previously been applied to several dye molecules and small biomolecules. However, to the best of our knowledge, this is the first report studying two structurally large and clinically important protein biomarkers, thyroglobulin (Tg) and myoglobin (Mb), using the GERS technique. In the GERS technique, if the excitation laser wavelength lies within the absorption band of the proteins, then this technique can be called graphene-enhanced resonance Raman scattering (GERRS).

For the first time, this paper aims to demonstrate the role of the GERS technique in significantly enhancing the Raman signal of two crucial protein biomarkers: Tg and Mb at low concentrations. The accurate and sensitive detection of Tg and Mb in biological samples is critical for the early diagnosis, prognosis, and treatment monitoring in life-threatening conditions.[41–44] Tg is a large glycoprotein produced by the thyroid gland, and it has a dimeric structure consisting of two identical polypeptide chains.[45,46] It serves as a precursor in the biosynthesis of thyroid hormones, such as triiodothyronine (T3) and thyroxine (T4), where iodination of tyrosine residues occurs.[47,48] In clinical diagnostics, the Tg levels are set as biomarkers for thyroid disorders, including thyroid cancer and autoimmune conditions like Hashimoto's thyroiditis.[49,50]

Mb is a protein found in the heart and skeletal muscles and is an important biomarker for the early diagnosis and assessment of myocardial infarction (heart attack).[44,51] It consists of 154 amino acids, including two histidine groups that interact with the iron atom in the heme prosthetic group.[43,52,53] Mb plays a crucial role in the storage and transport of oxygen in muscle tissues, especially during intense physical activity. The level of Mb in the blood is important for evaluating cardiac health and diagnosing muscle injuries.[44,54] Reliable detection of these biomarkers in biological samples such as blood or tissue enables significant progress in clinical diagnostics.

Herein, we report (i) the experimental arrangement for recording the conventional Raman scattering (CRS) and GERS spectra of Tg and Mb, (ii) the Raman spectra of bare MGF-based substrates, (iii) the GERS spectra of Tg and Mb recorded by probing at different locations, (iv) the assignment of all observed vibrational modes, and (iv) the absorption spectra of Tg and Mb solutions.

2. Materials and methods

2.1. Materials

The Tg from bovine thyroid (≥90% purity, product number: T1001) and Mb from equine heart (≥90% purity, product number: M1882) were sourced from Sigma-Aldrich, USA. Additionally, the monolayer graphene film (MGF), grown on copper foil through chemical vapor deposition (CVD), was also obtained from Sigma-Aldrich, USA (product number: 900415-1EA). The Tg and Mb protein solutions with a concentration of 10^{-6} M are separately prepared using deionized water as the solvent.

2.2. UV-visible spectroscopy of protein solutions

To assess the purity of the protein solutions and determine the appropriate laser wavelength for Raman scattering, we initially measured the absorption spectra of the protein solutions using a dual-beam UV-visible spectrophotometer (JASCO V-770).

2.3. CRS spectroscopy of Tg and Mb proteins

To record the CRS spectra of protein molecules, 10 μL of Tg and Mb solutions were drop-cast separately onto two different glass substrates using a micropipette. The samples were then allowed to dry completely at room temperature. The protein molecules dispersed on glass substrates were loaded into the Raman microscope (SekiTech, STR-750). The Ar^+ laser of wavelength 514 nm was directly focused on the glass substrate with the help of a 50× microscopic objective lens of numerical aperture (NA) 0.75. The Raman signal was collected in the back-scattering geometry using the combination of a 0.750 m imaging triple grating monochromator (Princeton Instruments Acton SP2750i, spectral resolution: 1.3 cm^{-1} with 600 grooves per mm) and a charge-coupled device camera (PIXIS-256E). The CRS spectra of Tg and Mb were recorded at different locations on glass substrates. However, no significant Raman signals from these proteins were detected. This suggests a possible limitation of the CRS technique in capturing the Raman signals of proteins on a glass substrate.

2.4. Preparation of MGF-based substrates

To obtain significant Raman signals, the GERS technique is used, with two different MGF-based substrates prepared for both proteins. For the preparation of the MGF-based substrate, we utilized the MGF grown on Cu foil through chemical vapor deposition (CVD), which was purchased from Sigma Aldrich, USA. The theoretically estimated thickness of MGF is 0.345 nm, with a transparency greater than 97%. For optimal sensing applications, the MGF must be undamaged, continuous, and devoid of any cracks or tears. Moreover, in order to improve the S/N, the MGF from Cu must be transferred to a glass substrate. Several techniques for transferring the MGF

from Cu to a glass substrate are documented in the literature.[16,55–59] However, for this study, we followed the method used in our previous work.[16] Some details of this method are as follows. A thin layer of polymethyl methacrylate (PMMA) was drop-cast on the MGF supported by a small rectangular-shaped 2 cm × 2 cm Cu foil. After completely drying, the MGF supported by PMMA and Cu on either side was transferred to 15% HNO_3 solution for complete etching of Cu. Afterward, the PMMA layer covering the MGF was fished out on a clean glass substrate and then soaked in hot acetone to wash away the PMMA layer. This left a clean MGF on the glass substrate, which was used as a GERS substrate for the proteins.

2.5. Characterization of MGF-based substrates

Before recording the GERS spectra of protein molecules, the MGF-based substrates were characterized by a Raman microscope and an atomic force microscope (AFM). The obtained Raman spectra are shown in the next section. Fig. S1, in the ESI,† represents a typical AFM image of the MGF placed on a glass slide displaying a smooth surface with a few surface contaminants. In a 200 nm × 200 nm AFM image of the MGF, the root mean square (RMS) roughness is 1.2 nm and the average roughness is 0.9 nm, respectively.

2.6. GERS spectroscopy of Tg and Mb proteins

After the characterization of MGF-based substrates, the Tg and Mb protein molecules were dispersed on two different MGF-based substrates by drop-casting 10 μL of protein solutions with a concentration of 10^{-6} M and allowing them to dry at room temperature. The protein molecules containing MGF-based substrates were loaded into the Raman microscope, and the spectra of both protein molecules were recorded using the same laser and microscopic objective lens (Fig. 1). Several Raman spectra were recorded by probing different locations on the MGF-based substrates containing the protein molecules.

3. Results and discussion

3.1. Absorption spectra of Raman probe molecules

As mentioned in the experimental details, the absorption spectra of the Tg and Mb solutions are recorded and shown in Fig. 2 to check their purity and absorption band. In general, the absorption band helps us to determine the suitable excitation wavelength for resonance Raman spectral measurements of the protein molecules. From Fig. 2, it is clear that the absorption spectra of Tg and Mb extend from ultraviolet to the visible region. The strong absorption in the ultraviolet region is primarily due to the presence of peptide bonds and aromatic amino acids in the protein molecules, highlighting their unique biochemical properties.[60–63] The GERS spectra of Tg and Mb protein molecules are obtained with an Ar^+ laser of wavelength 514 nm. It is noteworthy that the Tg and Mb protein solutions do not exhibit strong resonance at 514 nm, which is clear from Panels (a) and (b) of Fig. 2. There is no observable transition band of the proteins that is enhanced due to the resonance with an excitation wavelength of 514 nm. Consequently, the resonance effect seems not to be prominent. Therefore, the enhancement of the Raman signal for these proteins is primarily attributed to the GERS technique, while

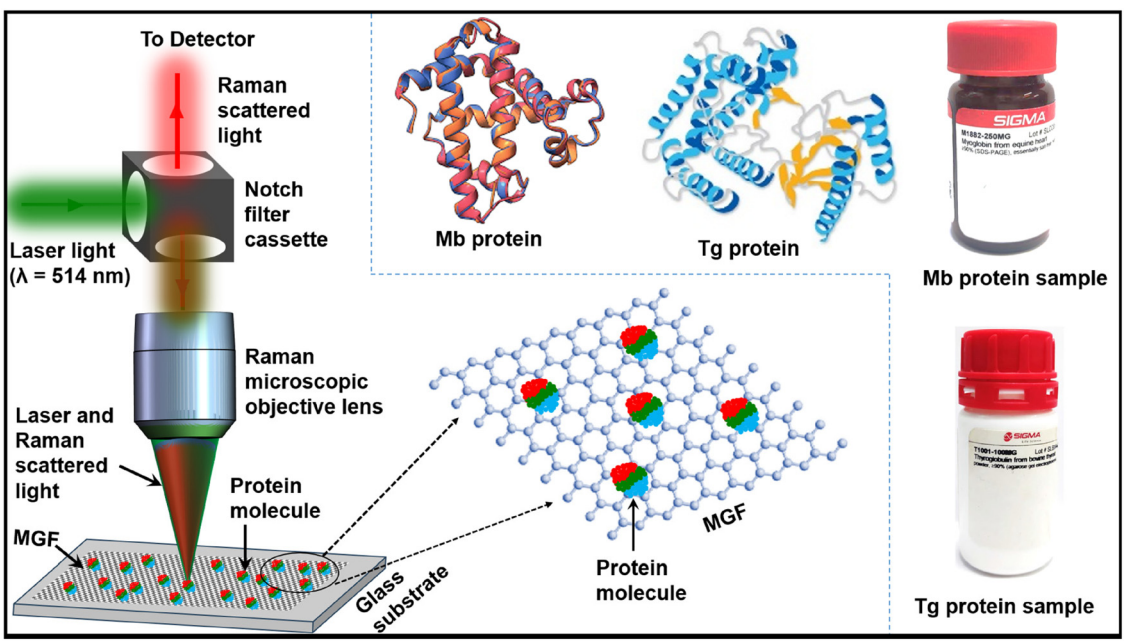

Fig. 1 Illustration of an experimental setup for recording the Raman spectra of protein molecules dispersed over the MGF-based substrate. A small portion of the substrate containing protein molecules is zoomed in and shown as an inset for better clarity. The ribbon diagrams and commercially available Mb and Tg samples are also shown in the inset.

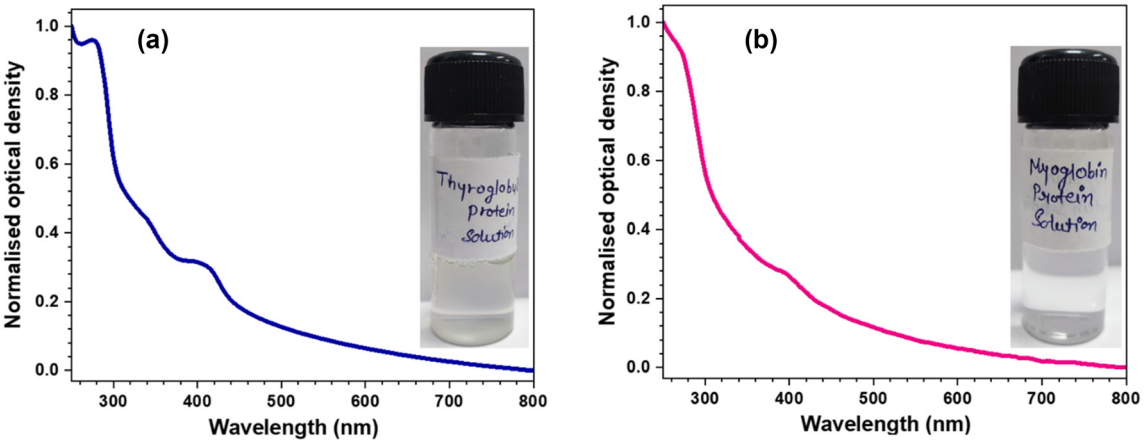

Fig. 2 Panels (a) and (b) represent the normalized absorption spectra of Tg and Mb solutions with a concentration of 1 μM, respectively. The protein solutions are shown in the insets of these panels.

the GERRS technique does not play a major role. It is also observed from Panels (a) and (b) of Fig. 2 that the Tg and Mb protein solutions show similarities in their absorption behavior. However, the absorption spectra of these proteins are slightly different from the ones reported in the literature.[64,65] These differences may result from the variation in the solvent or surrounding medium.

3.2. GERS spectra of Tg

As mentioned above, several CRS spectra of Tg are recorded by probing different locations. A typical CRS spectrum of Tg is shown in Panel (g) of Fig. 3. However, no significant vibrational modes are observed in this spectrum. This raises the demand for their GERS spectra to be recorded. Panels (a)–(e) of Fig. 3 represent a few GERS spectra of Tg obtained at different probed locations. To distinguish the vibrational modes of Tg protein molecules from the three fundamental modes of MGF-D (1350 cm^{-1}), G (1580 cm^{-1}), and 2D (2700 cm^{-1}) peaks, a typical Raman spectrum of MGF is displayed in Panel (f) of Fig. 3. The G band originates from a single resonance process associated with doubly degenerate in-plane transverse optical (iTO) and longitudinal optical (LO) phonon modes at the Brillouin zone center, while the 2D band is related to the two-phonon intervalley double resonance scattering involving iTO phonons near the K point. The D band is known as the disorder or defective band, and it originates from a double resonance Raman process involving the intervalley scattering of iTO phonons near the K point.[16] The intensity ratio of 2D and G peaks (I_{2D}/I_G), that is greater than 1.5 for the present case, clearly depicts the monolayer characteristic of the graphene film.[66] The spectra presented in these panels demonstrate a notable enhancement in the vibrational modes of Tg when they interact with the MGF-based substrate. This observation suggests that the presence of the MGF-based substrate significantly influences the molecular dynamics of the Tg protein and provides valuable insights into the interaction mechanisms between the Tg proteins and the MGF, highlighting the importance of a substrate in modulating protein activity. Here, the origin of enhancement is mainly supported by the chemical mechanism rather than the electromagnetic mechanism. In some GERS spectra of Tg, the vibrational modes of the MGF are entirely invisible, which indicates the efficient charge transfer from the MGF to Tg. The GERS spectra are found to strongly depend upon the probed location, as in the case of dye molecules,[16] because the charge transfer depends upon the orientation of the proteins on the MGF surface and which part of the protein is in physical contact with the MGF. Similar to the case of dye molecules as reported in the literature,[16] the vibrational mode widths are quenched by the MGF, resulting in sharp Raman peaks of Tg [Panel (a)].

It is worth noting that the significant improvement in the intensity of the vibrational modes of the MGF is reported in the presence of some Raman probe molecules due to the charge transfer from the Raman probe molecules to the MGF. However, this is not observed in the case of the MGF–Tg system. As mentioned earlier, the composition of Tg is notably rich in tyrosine and comprises a large number of amino acids. Additionally, it features extensive glycosylation, which involves the attachment of carbohydrate molecules to proteins. The modes identified in the GERS spectra of Tg protein molecules, based on their composition, are summarized in Table 1.

3.3. GERS spectra of Mb

Before recording the GERS spectra of Mb, the CRS spectra of Mb protein molecules are recorded by probing different locations. A typical CRS spectrum of Mb is shown in Panel (g) of Fig. 4. However, there are no significant vibrational modes in this spectrum. To investigate the vibrational modes of Mb on a bare glass slide, we used a higher concentration solution of Mb at 10 mM. Despite this increased concentration, no significant vibrational modes are observed, as shown in Panel (h) of Fig. 4. Panels (a)–(e) of Fig. 4 represent the GERS spectra of Mb obtained at different probed locations. All these spectra

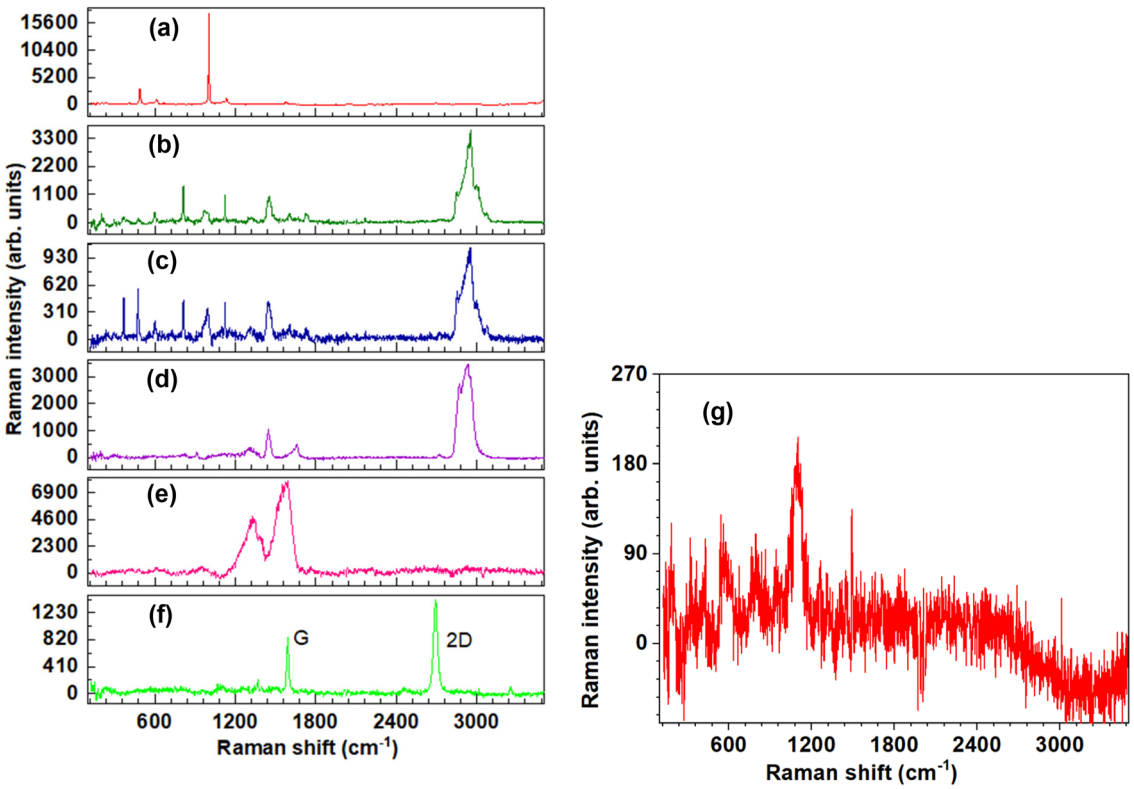

Fig. 3 Panels (a)–(e) depict the GERS spectra of Tg obtained by probing different locations. Panel (f) represents the Raman spectrum of a bare MGF-based substrate taken before dispersing the Tg. Panel (g) shows the CRS spectrum of the Tg protein molecules dispersed over the bare glass substrate.

Table 1 The assignment of observed vibrational modes in the GERS spectra of Tg, shown in Fig. 3. The vibrational mode assignment has been sourced from ref. 67–70

S. no.	Observed Raman shift (cm^{-1})	Vibration mode assignment
1	294	Skeletal deformation in D-glucose
2	476	Disulfide stretching vibration
3	410, 490	Ring deformation or skeletal mode in a D-glucose shoulder
4	667	Aromatic ring deformation
5	815	C–O–C stretching in a glycosidic bond
6	950–990	Skeletal stretching mode of the backbone or side chain of amino acids
7	1004	Phenylalanine vibration
8	1096–1160	C–O stretching vibration in D-glucose
9	1290–1300	Amide III band
10	1345	C–C stretching in tyrosine residues
11	1436–1470	C–H bending vibration in D-glucose
12	1580	Amide II band
13	1605–1657	Amide I (alpha-helical configuration)
14	2852	Symmetric and asymmetric bands of methylene bands
15	2938	Symmetric and asymmetric methyl bands
16	2993	Methine CH
17	3074	Aromatic CH

are different from the one recorded for the bare MGF-based substrate shown in Panel (f). In Panels (a)–(e), the vibrational modes of Mb are enhanced significantly in the presence of an MGF due to the chemical mechanism or charge transfer from the MGF to Mb. Here, the GERS spectra are also strongly dependent upon the probed location due to the reasons mentioned above. The reversible charge transfer is not observed in the MGF–Mb system as in the case of the MGF–Tg system.

Mb is made up of a diverse range of amino acids and includes histidine residues that are crucial for its function. It also contains heme prosthetic groups, which are organic compounds that help with the binding and release of oxygen. The distinct vibrational modes corresponding to various components of Mb are detailed in Table 2, offering insights into their structural and functional characteristics.

It is worth noting that from the Raman spectra of the MGF that is used as the GERS substrate for Tg and Mb protein solutions (Panels (f) of Fig. 3 and 4), it is clear that there is no significant peak at 1620 cm^{-1} and 2940 cm^{-1}. Also, the I_D/I_G is 0.2 in both cases. Therefore, we can easily conclude that there is no significant contribution from the structural factors such as defects and nanocrystalline grain boundaries.[75,76] It seems that the variation in the intensity of different Raman peaks in the GERS spectra is due to the different protein orientations at various locations, as mentioned above. Based on the vibrational modes observed in the GERS spectra of Tg and Mb, the possible orientations of these proteins are estimated and summarized in Tables S1 and S2 in the ESI.†

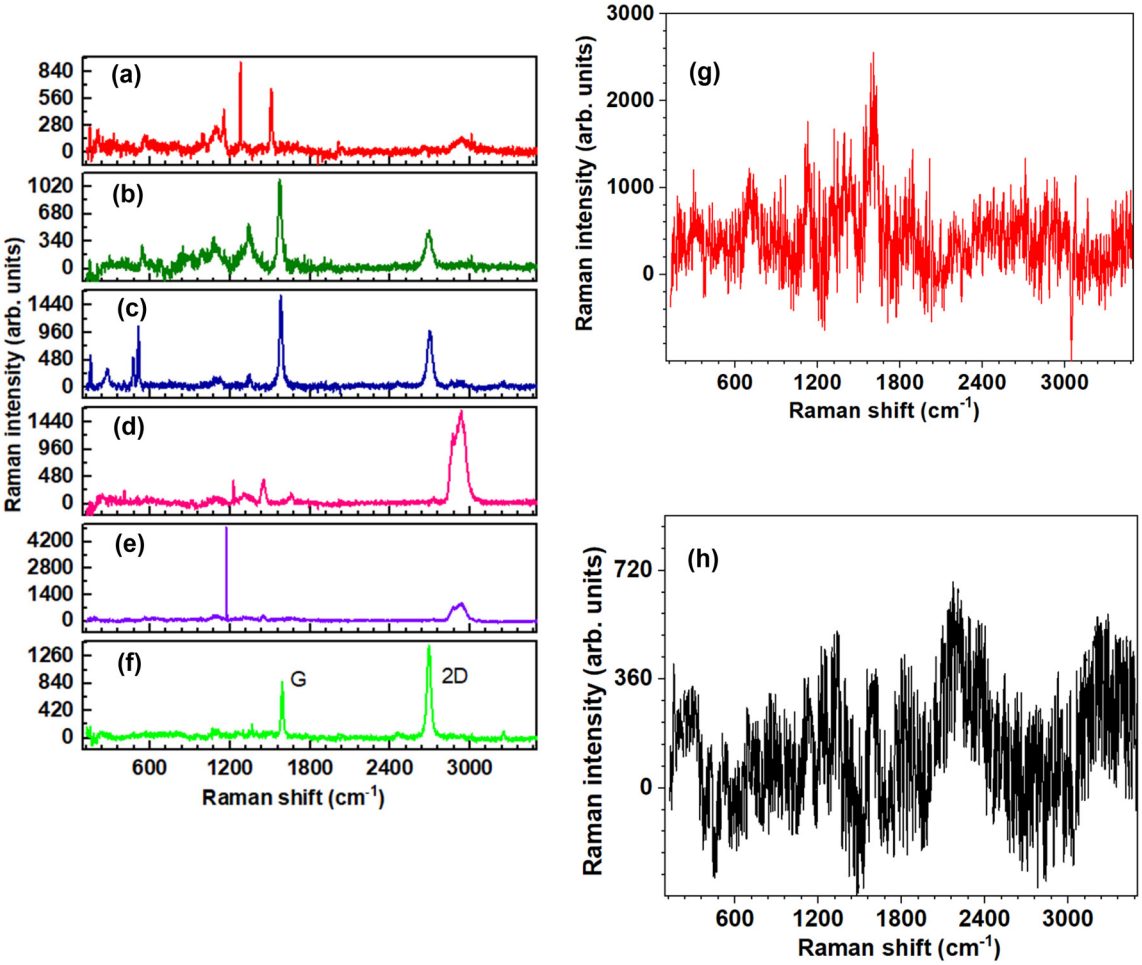

Fig. 4 Panels (a)–(e) represent the Raman spectra of Mb protein molecules dispersed on an MGF-based substrate, obtained by probing different locations on their surface. The Raman spectrum of a bare MGF-based substrate is taken before dispersing the Mb protein, shown in Panel (f). Panels (g) and (h) represent the CRS spectra of MB protein molecules dispersed over glass substrates by drop-casting 10 ml of Raman probe solutions with concentrations of 1 μM and 10 mM, respectively.

Table 2 The assignment of observed vibrational modes in the GERS spectra of Mb protein molecules, shown in Fig. 4. The vibrational mode assignment has been sourced from ref. 70–74

S. no.	Observed Raman shift (cm^{-1})	Vibration mode assignment
1	220–240	Fe–His stretching vibration
2	474	Low frequency heme group vibration
3	512	Fe–N stretching vibration
4	540–572	Fe–O stretching vibration
5	848	Ring breathing mode in tyrosine residue
6	997	Ring breathing mode of phenylalanine residue
7	1098	C–N stretching in the porphyrin ring
8	1150–1170	In-plane skeletal deformation of the porphyrin ring
9	1226	Amide III band (beta sheet configuration)
10	1283	Amide III band (alpha helical configuration)
11	1338	Amide III band
12	1353	In-plane bending vibration of the porphyrin ring (weak)
13	1454–1466	C=C and C–N bonds in the porphyrin ring
14	1509	Porphyrin ring high frequency mode
15	1554	Skeletal deformation mode
16	1580–1585	C=C stretching vibration of the porphyrin ring
17	1627–1640	In-plane bending vibration of the porphyrin ring (moderate)
18	1656	Amide I (alpha helical configuration)
19	2874	Symmetric and asymmetric methylene bands
20	2876	Histidine CH_2 group
21	2930	Symmetric and asymmetric methyl bands

In the present experiment, we used a laser power of 1 mW with a minimal exposure time of 5 seconds, which prevents protein denaturation. Also, our earlier research noted a similar location-dependent enhancement in the GERS spectrum of dye molecules, as detailed in ref. 16. Different orientations of proteins at various locations can activate distinct vibrational modes. Although not all vibrational modes are active simultaneously, recording a few spectra from nearby locations allows us to capture all possible vibrational modes. Therefore, we still believe that the GERS technique can be utilized for sensing protein biomarkers.

4. Conclusions

The Tg and Mb solutions were prepared, and their absorption spectra were recorded. From these spectra, it was found that their absorption bands ranged from ultraviolet to visible regions. The CRS spectra of these proteins were recorded by drop-casting these proteins on glass substrates. However, no significant vibrational modes were found in these spectra. Later, the MGFs were transferred successfully from the Cu substrate to the glass substrate using a chemical route and characterized using Raman spectroscopy as a tool. Using the MGF-based substrates, the GERS spectra of these proteins were recorded with a high S/N ratio by focusing the laser light at different locations. Based on the S/N ratio observed in the GERS spectra of Tg and Mb protein molecules, we can easily conclude that this technique can be utilized further for samples of lower concentrations than μM. In both cases, the several vibrational modes were significantly enhanced through the irreversible charge transfer process from MGFs to proteins. The number and intensity of the vibrational modes in the GERS spectra of these proteins were found to be very sensitive to the probed location. All the observed modes are assigned. It is to be noted that there has been no report on the GERS of Tg and Mb to date. Therefore, this will be the first report dealing with the GERS of Tg and Mb. The present experimental study revealed that several vibrational modes of these proteins are Raman active. From the observed S/N ratio of the vibrational modes, we easily conclude that the GERS technique will be a useful tool for detecting Tg and Mb at their low concentrations, and this will help us to diagnose dangerous diseases related to the thyroid and heart at an early stage. The results obtained pave the way for sensing applications by extending to other essential enzymes, biomolecules, and pesticides, offering a more detailed understanding of molecular constituents. This approach enhances our comprehension of the chemical mechanisms behind Raman signal enhancement and the interactions of molecules with the graphene surface. Given these impressive outcomes, this technique can be integrated with other plasmonic and photonic nanostructures, leading to the development of portable sensing devices capable of detecting probe molecules in their native state, even at ultralow concentrations.

Author contributions

Anamika Sharma: writing – review & editing, writing – original draft, visualization, validation, methodology, investigation, formal analysis, data curation, and conceptualization. Venkata Ramanaiah Dantham: writing – review & editing, writing – original draft, visualization, supervision, and conceptualization.

Conflicts of interest

There are no conflicts to declare.

Data availability statement

The data that support the findings of this study are available from the corresponding author upon reasonable request.

Acknowledgements

The authors acknowledge the Science and Engineering Research Board (SERB), Government of India, under Grant CRG/2021/002951 and EEQ/2023/000876, and the DST, Government of India, for the research grant number SR/FST/PS-1/2018/34(C).

References

1 A. A. Bunaciu, H. Y. Aboul-Enein and V. D. Hoang, *Appl. Spectrosc. Rev.*, 2015, **50**, 377–386.
2 L. M. Moreira, L. Silveira, F. V. Santos, J. P. Lyon, R. Rocha, R. A. Zângaro, A. B. Villaverde and M. T. T. Pacheco, *Spectroscopy*, 2008, **22**, 1–19.
3 H. J. Butler, L. Ashton, B. Bird, G. Cinque, K. Curtis, J. Dorney, K. Esmonde-White, N. J. Fullwood, B. Gardner, P. L. Martin-Hirsch, M. J. Walsh, M. R. McAinsh, N. Stone and F. L. Martin, *Nat. Protoc.*, 2016, **11**, 664–687.
4 Y. Bai, Z. Yu, S. Yi, Y. Yan, Z. Huang and L. Qiu, *J. Pharm. Biomed. Anal.*, 2020, **190**, 113514.
5 N. Kuhar, S. Sil and S. Umapathy, *Spectrochim. Acta, Part A*, 2021, **258**, 119712.
6 N. Kuhar, S. Sil, T. Verma and S. Umapathy, *RSC Adv.*, 2018, **8**, 25888–25908.
7 J. Smulko, M. S. Wrobel and I. Barman, in *2015 International Conference on Noise and Fluctuations, ICNF 2015*, 2015, pp. 1–6.
8 S. Huang, R. Pandey, I. Barman, J. Kong and M. Dresselhaus, *ACS Photonics*, 2018, **5**, 2978–2982.
9 C. Song, S. Guo, S. Jin, L. Chen and Y. M. Jung, *Chemosensors*, 2020, **8**, 118.
10 K. V. Sreekanth, J. Perumal, U. S. Dinish, P. Prabhathan, Y. Liu, R. Singh, M. Olivo and J. Teng, *Nat. Commun.*, 2023, **14**, 7085.

11 G. M. Das, R. Laha and V. R. Dantham, *J. Raman Spectrosc.*, 2016, **47**, 895–900.
12 G. M. Das, A. B. Ringne, V. R. Dantham, R. K. Easwaran and R. Laha, *Opt. Express*, 2017, **25**, 19822–19831.
13 A. Sharma and V. R. Dantham, *Spectrochim. Acta, Part A*, 2023, **297**, 122736.
14 S. Frustaci and F. Vollmer, *Curr. Opin. Chem. Biol.*, 2019, **51**, 66–73.
15 S. Stewart and P. M. Fredericks, *Spectrochim. Acta, Part A*, 1999, **55**, 1641–1660.
16 A. Sharma and V. R. Dantham, *Spectrochim. Acta, Part A*, 2024, **317**, 124431.
17 H. Ma, S. Yan, X. Lu, Y. F. Bao, J. Liu, L. Liao, K. Dai, M. Cao, X. Zhao, H. Yan, H. L. Wang, X. Peng, N. Chen, H. Feng, L. Zhu, G. Yao, C. Fan, D. Y. Wu, B. Wang, X. Wang and B. Ren, *Sci. Adv.*, 2023, **9**, eadh8362.
18 X. Ling, L. G. Moura, M. A. Pimenta and J. Zhang, *J. Phys. Chem. C*, 2012, **116**, 25112–25118.
19 L. Xie, X. Ling, Y. Fang, J. Zhang and Z. Liu, *J. Am. Chem. Soc.*, 2009, **131**, 9890–9891.
20 X. Ling, J. Wu, W. Xu and J. Zhang, *Small*, 2012, **8**, 1365–1372.
21 X. Ling, J. Wu, L. Xie and J. Zhang, *J. Phys. Chem. C*, 2013, **117**, 2369–2376.
22 X. Ling and J. Zhang, *Small*, 2010, **6**, 2020–2025.
23 S. Huang, X. Ling, L. Liang, Y. Song, W. Fang, J. Zhang, J. Kong, V. Meunier and M. S. Dresselhaus, *Nano Lett.*, 2015, **15**, 2892–2901.
24 X. Ling, W. Fang, Y. H. Lee, P. T. Araujo, X. Zhang, J. F. Rodriguez-Nieva, Y. Lin, J. Zhang, J. Kong and M. S. Dresselhaus, *Nano Lett.*, 2014, **14**, 3033–3040.
25 X. Ling, L. Xie, Y. Fang, H. Xu, H. Zhang, J. Kong, M. S. Dresselhaus, J. Zhang and Z. Liu, *Nano Lett.*, 2010, **10**, 553–561.
26 A. Armano and S. Agnello, *C*, 2019, **5**, 67.
27 S. A. Ghopry, B. Liu, A. Shultz and J. Z. Wu, *ACS Appl. Nano Mater.*, 2023, **6**, 21626–21633.
28 G. Faggio, R. Grillo, N. Lisi, F. Buonocore, R. Chierchia, M. J. Kim, G. H. Lee, A. Capasso and G. Messina, *Appl. Surf. Sci.*, 2022, **599**, 154035.
29 P. Kaushik, F. J. Sonia, G. Haider, M. K. Thakur, V. Valeš, J. Kong and M. Kalbáč, *Adv. Mater. Interfaces*, 2022, **9**, 2200478.
30 X. Ling, S. Huang, S. Deng, N. Mao, J. Kong, M. S. Dresselhaus and J. Zhang, *Acc. Chem. Res.*, 2015, **48**, 1862–1870.
31 E. L. Brightbill, K. T. Young, H. F. Gezahagne, D. S. Jin, B. Hitchcock and E. M. Vogel, *2D Mater.*, 2021, **8**, 025015.
32 H. Lai, F. Xu, Y. Zhang and L. Wang, *J. Mater. Chem. B*, 2018, **6**, 4008–4028.
33 Y. Cao, Y. Cheng and M. Sun, *Appl. Spectrosc. Rev.*, 2023, **58**, 1–38.
34 V. Kaushik, H. L. Kagdada, D. K. Singh and S. Pathak, *Appl. Surf. Sci.*, 2022, **574**, 151724.
35 W. Xu, X. Ling, J. Xiao, M. S. Dresselhaus, J. Kong, H. Xu, Z. Liu and J. Zhang, *Proc. Natl. Acad. Sci. U. S. A.*, 2012, **109**, 9281–9286.
36 W. Xu, N. Mao and J. Zhang, *Small*, 2013, **9**, 1206–1224.
37 S. Thakkar, L. De Luca, S. Gaspa, A. Mariani, S. Garroni, A. Iacomini, L. Stagi, P. Innocenzi and L. Malfatti, *ACS Omega*, 2022, **7**, 5670–5678.
38 A. Silver, H. Kitadai, H. Liu, T. Granzier-Nakajima, M. Terrones, X. Ling and S. Huang, *Nanomaterials*, 2019, **9**, 516.
39 G. Sarau, C. Daniel, M. Heilmann, G. Leuchs, K. Amann and S. H. Christiansen, *Adv. Mater. Technol.*, 2021, **6**, 2100385.
40 Y. Shao, J. Wang, H. Wu, J. Liu, I. A. Aksay and Y. Lin, *Electroanalysis*, 2010, **22**, 1027–1036.
41 I. Đorić and S. Šelemetjev, *Bioanalysis*, 2024, **16**, 49–60.
42 E. Antonini, *Physiol. Rev.*, 1965, **45**, 123–170.
43 O. Bangcharoenpaurpong, K. T. Schomacker and P. M. Champion, *J. Am. Chem. Soc.*, 1984, **106**, 5688–5698.
44 W. A. El-Said, D. M. Fouad and S. A. El-Safty, *Sens. Actuators, B*, 2016, **228**, 401–409.
45 J. Der Lin, *Clin. Chim. Acta*, 2008, **388**, 15–21.
46 E. Jeong, J. K. Yoon, S. J. Lee, E. Y. Soh, J. Lee, H. K. Kim and Y. S. An, *Medicine*, 2019, **98**, e18437.
47 J. T. Dunn and A. D. Dunn, *Biochemistry*, 1999, **81**, 505–509.
48 C. E. Citterio, H. M. Targovnik and P. Arvan, *Nat. Rev. Endocrinol.*, 2019, **15**, 323–338.
49 Y. Nagayama, *Horm. Metab. Res.*, 2018, **50**, 922–931.
50 S. Santhoshkumar, U. Ramasamy, R. F. Mansuour and E. Ramaraj, in *Proceedings of the Confluence 2021: 11th International Conference on Cloud Computing, Data Science and Engineering*, 2021, pp. 1040–1045.
51 S. K. Asl and M. Rahimzadegan, *J. Pharm. Biomed. Anal.*, 2022, **211**, 114624.
52 R. Eslami-Farsani, S. Farhadian, B. Shareghi and S. Asgharzadeh, *J. Mol. Liq.*, 2022, **352**, 118691.
53 J. P. Collman and L. Fu, *Acc. Chem. Res.*, 1999, **32**, 455–463.
54 M. Plebani and M. Zaninotto, *Clin. Chim. Acta*, 1998, **272**, 69–77.
55 X. Li, Y. Zhu, W. Cai, M. Borysiak, B. Han, D. Chen, R. D. Piner, L. Colomba and R. S. Ruoff, *Nano Lett.*, 2009, **9**, 4359–4363.
56 C. T. Cherian, F. Giustiniano, I. Martin-Fernandez, H. Andersen, J. Balakrishnan and B. Özyilmaz, *Small*, 2015, **11**, 189–194.
57 Z. Wu, Y. Guo, Y. Guo, R. Huang, S. Xu, J. Song, H. Lu, Z. Lin, Y. Han, H. Li, T. Han, J. Lin, Y. Wu, G. Long, Y. Cai, C. Cheng, D. Su, J. Robertson and N. Wang, *Nanoscale*, 2016, **8**, 2594–2600.
58 M. Kim, A. Shah, C. Li, P. Mustonen, J. Susoma, F. Manoocheri, J. Riikonen and H. Lipsanen, *2D Mater.*, 2017, **4**, 035004.
59 G. Deokar, J. Avila, I. Razado-Colambo, J. L. Codron, C. Boyaval, E. Galopin, M. C. Asensio and D. Vignaud, *Carbon*, 2015, **89**, 82–92.
60 S. Prasad, I. Mandal, S. Singh, A. Paul, B. Mandal, R. Venkatramani and R. Swaminathan, *Chem. Sci.*, 2017, **8**, 5416–5433.

61 M. A. Saraiva, *J. Photochem. Photobiol., B*, 2020, **212**, 112022.
62 J. M. Antosiewicz and D. Shugar, *Biophys. Rev.*, 2016, **8**, 163–177.
63 L. A. Ginsel, *Biochem. J.*, 1939, **33**, 428.
64 A. Van Zyl and H. Edelhoch, *J. Biol. Chem.*, 1967, **242**, 2423–2427.
65 A. J. Atkin, J. M. Lynam, B. E. Moulton, P. Sawle, R. Motterlini, N. M. Boyle, M. T. Pryce and I. J. S. Fairlamb, *Dalton Trans.*, 2011, **40**, 5755–5761.
66 Y. Gui, H. Sun, H. Yan, H. Wang, Y. Zhang, X. M. Song and R. Jia, *Solid State Commun.*, 2017, **264**, 31–34.
67 A. L. Jenkins, R. A. Larsen and T. B. Williams, *Spectrochim. Acta, Part A*, 2005, **61**, 1585–1594.
68 S. Stewart and P. M. Fredericks, *Spectrochim. Acta, Part A*, 1999, **55**, 1641–1660.
69 G. Zhu, X. Zhu, Q. Fan and X. Wan, *Spectrochim. Acta, Part A*, 2011, **78**, 1187–1195.
70 T. M. Theophanides, ed. *Infrared and Raman Spectroscopy of Biological Molecules*, NATO Advanced Study Institutes Series, Springer, Dordrecht, The Netherlands, 1979, Vol. 43.
71 F. Adar, N. Zheng, Z. Wang, F. Zhao, H. Li, H. He, G. Wang and H. Sheng, *Spectroscopy*, 2022, **37**, 9–13.
72 A. Rygula, K. Majzner, K. M. Marzec, A. Kaczor, M. Pilarczyk and M. Baranska, *J. Raman Spectrosc.*, 2013, **44**, 1061–1076.
73 S. Hu, K. M. Smith and T. G. Spiro, *J. Am. Chem. Soc.*, 1996, **118**, 12638–12646.
74 S. S. Sibbett, S. J. Klebanoff and J. K. Hurst, *FEBS Lett.*, 1985, **189**, 271–275.
75 T. Zhou, C. Xu and W. Ren, *Nano Lett.*, 2022, **22**, 9380–9388.
76 G. Faggio, G. G. Politano, N. Lisi, A. Capasso and G. Messina, *J. Phys.: Condens. Matter*, 2024, **36**, 195303.